Journal of
Radiation Protection and Research 2022;47(3):158–166
https://doi.org/10.14407/jrpr.2022.00052

pISSN 2508-1888 | eISSN 2466-2461

Bias-corrected $H_p(10)$-to-Organ-Absorbed Dose Conversion Coefficients for the Epidemiological Study of Korean Radiation Workers

Areum Jeong[1], Tae-Eun Kwon[2], Wonho Lee[3], Sunhoo Park[1]

[1]Department of Radiation Emergency Medicine, Korea Institute of Radiological and Medical Sciences, Seoul, Korea; [2]Division of Cancer Epidemiology and Genetics, National Cancer Institute, National Institute of Health, Rockville, MD, USA; [3]College of Health and Environmental Science, Korea University, Seoul, Korea

ABSTRACT

Background: The effects of radiation on the health of radiation workers who are constantly susceptible to occupational exposure must be assessed based on an accurate and reliable reconstruction of organ-absorbed doses that can be calculated using personal dosimeter readings measured as $H_p(10)$ and dose conversion coefficients. However, the data used in the dose reconstruction contain significant biases arising from the lack of reality and could result in an inaccurate measure of organ-absorbed doses. Therefore, this study quantified the biases involved in organ dose reconstruction and calculated the bias-corrected $H_p(10)$-to-organ-absorbed dose coefficients for the use in epidemiological studies of Korean radiation workers.

Materials and Methods: Two major biases were considered: (a) the bias in $H_p(10)$ arising from the difference between the dosimeter calibration geometry and the actual exposure geometry, and (b) the bias in air kerma-to-$H_p(10)$ conversion coefficients resulting from geometric differences between the human body and slab phantom. The biases were quantified by implementing personal dosimeters on the slab and human phantoms coupled with a Monte Carlo method and considered to calculate the bias-corrected $H_p(10)$-to-organ-absorbed dose conversion coefficients.

Results and Discussion: The bias in $H_p(10)$ was significant for large incident angles and low energies (e.g., 0.32 for right lateral at 218 keV), whereas the bias in dose coefficients was significant for the posteroanterior (PA) geometry only (e.g., 0.79 at 218 keV). The bias-corrected $H_p(10)$-to-organ-absorbed dose conversion coefficients derived in this study were up to 3.09-fold greater than those from the International Commission on Radiological Protection publications without considering the biases.

Conclusion: The obtained results will aid future studies in assessing the health effects of occupational exposure of Korean radiation workers. The bias-corrected dose coefficients of this study can be used to calculate organ doses for Korean radiation workers based on personal dose records.

Keywords: Conversion Coefficient, Organ-Absorbed Dose, Bias Quantification, Monte Carlo Method, Epidemiological Study

Original Research

Received April 26, 2022
Revision June 18, 2022
Accepted August 5, 2022

Corresponding author: Tae-Eun Kwon

National Institute of Health, 9609 Medical Center Drive, 7E412, Rockville, MD 20850, USA
E-mail: taeeun.kwon@nih.gov
https://orcid.org/0000-0002-7252-4634

Introduction

Radiation workers are constantly susceptible to occupational exposure. Thus, the assessment of the radiation effect on health has become important because of increasing

concerns about protracted exposure. Previous studies generally used the personal dose equivalent $H_p(10)$ to evaluate the health effects associated with occupational exposure. Similar to other countries, the occupational exposure of Korean radiation workers is managed in terms of $H_p(10)$, measured by personal dosimeters such as the thermoluminescent dosimeter (TLD), and the measured $H_p(10)$ values are reported every 3 months to the national dose registry.

However, to evaluate cancer morbidity and mortality, the International Commission on Radiological Protection (ICRP) strongly recommends the use of an organ-absorbed dose rather than $H_p(10)$ [1]. Unfortunately, it is impossible to directly measure organ-absorbed doses because dosimeters should not be inserted into the human body. For this reason, organ-absorbed doses for radiation workers should be derived from $H_p(10)$ values using dose conversion coefficients. The ICRP has provided the dose conversion coefficients for air kerma-to-$H_p(10)$ and air kerma-to-organ-absorbed doses calculated based on a 30 cm × 30 cm × 15 cm slab phantom (mass composition: 76.2% oxygen, 11.1% carbon, 10.1% hydrogen, and 2.6% nitrogen) and anthropomorphic phantoms coupled with Monte Carlo methods [2, 3], respectively. Accordingly, the organ-absorbed dose can be calculated by converting $H_p(10)$ using the aforementioned dose conversion coefficients.

However, several biases affect the reliability and validity of the risk assessment of occupational exposure in the reconstruction of the organ-absorbed dose. First, a bias in the recorded $H_p(10)$ occurs during the calibration and reading of personal dosimeters. Although personal dosimeters are practically exposed to radiation from various directions in addition to having different angular dependencies depending on the incident angle, the exposure geometry, except the anteroposterior (AP), is ignored in the existing calibration and reading procedure. In addition, the slab phantom used for calibration is not similar to the human body, where an actual personal dosimeter is positioned. Therefore, the accuracy of the recorded $H_p(10)$ varies with exposure conditions and calibration geometry. The calibration procedure of a personal dosimeter can introduce bias in the recorded $H_p(10)$ because the angular dependency and the differences between the slab phantom and the human body are not considered.

Furthermore, an important bias is introduced while deriving organ-absorbed doses from recorded $H_p(10)$ through the ICRP air kerma-to-$H_p(10)$ conversion coefficients. The ICRP air kerma-to-$H_p(10)$ conversion coefficients are derived from a cuboid slab phantom. However, in actual practice, $H_p(10)$ is measured using a personal dosimeter worn on a radiation worker's body, not a slab phantom. Therefore, differences exist between the actual measurement geometry of $H_p(10)$ and the slab phantom-based calibration geometry that are used to calculate the conversion coefficients. These differences introduce bias in the estimation of air kerma from recorded $H_p(10)$ and consequently affect the derivation of organ-absorbed doses. For example, for exposure from the postero-anterior (PA) direction, the attenuation thickness for the human body is typically expected to be higher than 200 mm, whereas that for a slab phantom is only 140 mm, according to the definition of $H_p(10)$. In this case, although the recorded $H_p(10)$ is measured after being attenuated by the human body, only the attenuation by the slab phantom is considered in the air kerma calculations. Therefore, the calculated air kerma is underestimated, which means that the organ-absorbed dose is underestimated. For these reasons, to improve the validity of the estimated organ-absorbed doses, it is necessary to analyze biases that affect dose conversions.

In this study, we attempted to quantify the biases introduced into the recorded $H_p(10)$ and subsequently into the slab phantom-based conversion coefficients (air kerma-to-$H_p(10)$) to finally derive the organ-absorbed dose for radiation workers. For this purpose, a Monte Carlo simulation of the dosimeter measurement coupled with the slab and the anthropomorphic phantoms was performed.

Materials and Methods

1. Background of Organ-Absorbed Dose Reconstruction

An organ-absorbed dose can be reconstructed from recorded $H_p(10)$ as follows:

$$D_T = H_p(10)\left[\frac{H_p(10)}{K_a}\right]^{-1}\left[\frac{D_T}{K_a}\right], \quad (1)$$

where D_T is the tissue or organ-absorbed dose (Gy); $H_p(10)$ is the personal dose equivalent at a depth of 10 mm (Sv); $H_p(10)/K_a$ is the air kerma-to-$H_p(10)$ conversion coefficient (Sv/Gy); and D_T/K_a is the air kerma-to-organ-absorbed dose conversion coefficient (Gy/Gy).

The two conversion coefficients (i.e., $H_p(10)/K_a$ and D_T/K_a) are determined according to the exposure scenarios (energy and geometry) to which radiation workers are exposed. ICRP $H_p(10)/K_a$ values calculated based on a slab phantom according to the photon energy and the incident angle are pro-

vided in Table A.24 of ICRP Publication 74 [2]. D_T/K_a can be calculated based on simulations using computational human phantoms. ICRP has provided reference D_T/K_a values calculated based on the ICRP reference voxel phantom [3]. Computation was performed according to idealized geometries: AP, PA, right lateral (RLAT), left lateral (LLAT), rotational (ROT), and isotropic (ISO) [3]. The cranial-caudal and caudal-cranial geometries introduced in the US National Council on Radiation Protection and Measurements (NCRP) report were also considered in this study [4].

2. Bias in Organ Dose Reconstruction

Two types of biases were considered in this study: the bias B_1 in the recorded $H_p(10)$ and the bias B_2 in $H_p(10)/K_a$. B_1 arises because the response of the personal dosimeter under the current calibration conditions (i.e., the irradiation in the AP direction and the use of the slab phantom) may differ that under the actual exposure conditions. Therefore, B_1 can be quantified using the ratio of the dosimeter response under the irradiation on the anthropomorphic phantom at the incident angle α to that under the irradiation on a slab phantom at 0°. In addition, the difference in reference $H_p(10)$ (i.e., the value used as the correction factor for calibration) introduced by the differences between the calibration geometry (AP) and actual exposure geometry is also considered.

$$B_1 = \left[\frac{R(E,\alpha)_{\text{human}}}{R(E,0^\circ)_{\text{slab}}}\right]\left[\frac{H_p(10;E,\alpha)_{\text{human}}}{H_p(10;E,0^\circ)_{\text{slab}}}\right]^{-1}, \quad (2)$$

where $R(E, \alpha)_{\text{human}}$ denotes the dosimeter response on the anthropomorphic phantom irradiated at an incident angle α; $R(E, 0°)_{\text{slab}}$ denotes the dosimeter response on the slab phantom irradiated at 0° (AP); $H_p(10; E, \alpha)_{\text{human}}$ denotes the $H_p(10)$ values depending on the actual exposure energy and geometry; and $H_p(10; E, 0°)_{\text{slab}}$ denotes the $H_p(10)$ values for AP geometry, which have been provided by ICRP. More specifically, to quantify the response R with Monte Carlo simulation, R was defined as the absorbed dose delivered to the element of the personal dosimeter per unit of air kerma.

Another bias, B_2, can also be quantified by comparing the conversion coefficients based on the anthropomorphic and slab phantoms. Because this bias involved in the dose conversion coefficients results from the geometric differences between the human body and the slab phantom, B2 is defined as follows:

$$B_2 = \left[\left(\frac{H_p(10)}{K_a}\right)_{\text{human}}\right]\left[\left(\frac{H_p(10)}{K_a}\right)_{\text{slab}}\right]^{-1}, \quad (3)$$

where $(H_p(10)/K_a)_{\text{human}}$ is the anthropomorphic phantom-based $H_p(10)/K_a$, and $(H_p(10)/K_a)_{\text{slab}}$ is the slab phantom-based $H_p(10)/K_a$, which have been provided by ICRP.

3. Monte Carlo Simulation for Bias Estimation

In the quantification of the biases, we used the Korean Typical Man-2 (KTMAN-2) computational phantom constructed from high-resolution anatomical images of Koreans to minimize the physical differences between Korean radiation workers and the anthropomorphic phantom. KTMAN-2 is a computed tomography image-based voxel phantom consisting of 300 × 150 × 344 voxels with a resolution of 2 mm × 2 mm × 5 mm [5]. KTMAN-2 was implemented based on the Monte Carlo N-Particle 6 (MCNP 6) code. The field size was defined as 50 cm × 60 cm for AP, PA, RLAT, and LLAT geometries and 60 cm × 80 cm for the cranial-caudal and caudal-cranial geometries; the size was considered sufficient to approximately model whole-body irradiation. In the LAT geometry (i.e., an incident angle of 90°), because a depth of 10 mm cannot be defined, the $H_p(10)$ value cannot be defined. Therefore, the response was calculated with an incident angle of 75° [4]. For the same reason, the cranial-caudal and caudal-cranial geometries were also exposed at 75°. The responses for ROT and ISO geometries were calculated by averaging those for four geometries (AP, PA, LLAT, and RLAT) and six geometries (AP, PA, LLAT, RLAT, cranial-caudal, and caudal-cranial), respectively.

To calculate B_1 from the relative response of a TLD, personal dosimeters on the slab and KTMAN-2 phantom (Fig. 1) were modeled after the Panasonic TLD UD-802 model (Panasonic Corporation, Tokyo, Japan), which is commonly used in radiation facilities in Korea. TLD UD-802 measured $H_p(10)$ using a 0.05-mm thick thermoluminescent material ($CaSO_4$) and a 1 g·cm^{-2} filter made of lead and plastic. The absorbed doses in the $CaSO_4$ element were calculated using the energy deposition (type F6) tally for AP, PA, RLAT, LLAT, cranial-caudal, and caudal-cranial geometries. Thus, the relative response was calculated as the ratio of the absorbed dose in the $CaSO_4$ element on the KTMAN-2 to that on the slab phantom. To confine the statistical error of the simulation result within 5%, 10^8–10^9 histories were used. The position of the personal dosimeter worn on the front was selected as 14.4 cm below the thyroid gland and 4 cm left from the midline, where it is commonly worn [6].

The bias estimation was performed for energies of 218, 397, and 662 keV, suggested as representative exposure ener-

https://doi.org/10.14407/jrpr.2022.00052

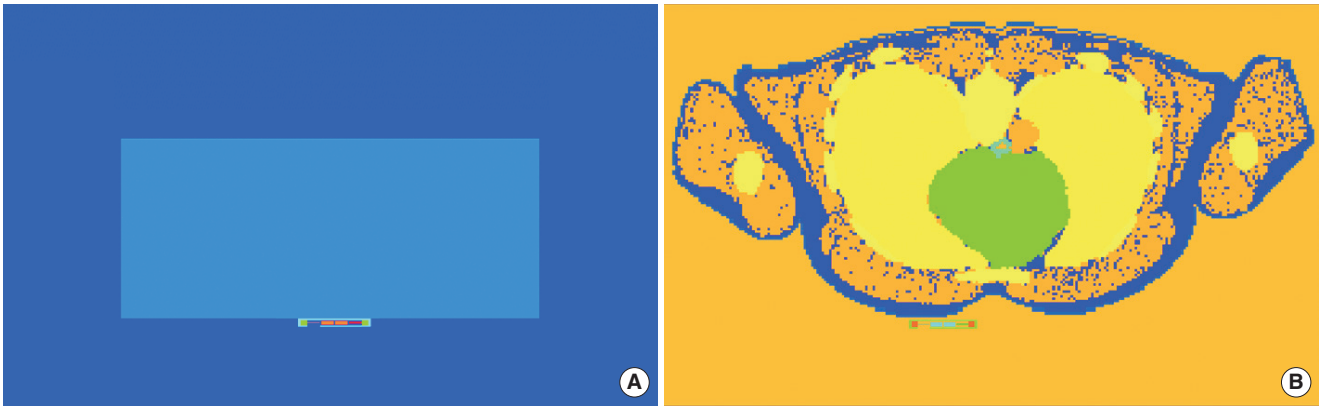

Fig. 1. Transverse plane images of personal dosimeter implemented in Monte Carlo N-Particle 6 (MCNP6) code for the calculation of B_1 with the slab phantom (A) and with Korean Typical Man-2 (KTMAN-2) (B).

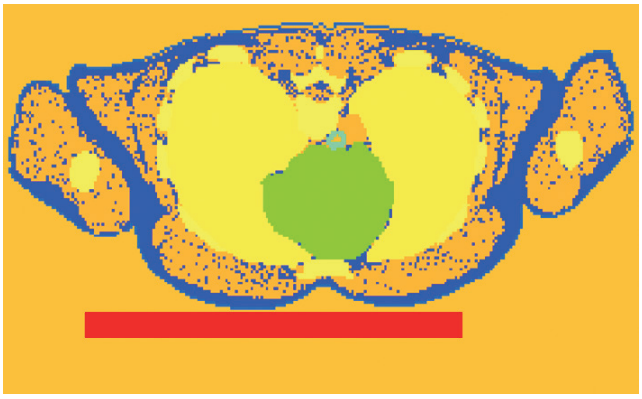

Fig. 2. Transverse plane image of cuboid tissue equivalent material (red) and Korean Typical Man-2 (KTMAN-2) implemented in Monte Carlo N-Particle 6 (MCNP6) code for the calculation of of $H_p(10; E, \alpha)_{human}$.

Table 1. Results of Verification for the Bias Estimation Method

Energy (MeV)	ICRP 74 (A)	This study (B)	Ratio (B/A)
0.03	1.11	1.13	1.01
0.04	1.49	1.51	1.01
0.05	1.77	1.79	1.01
0.06	1.89	1.90	1.00
0.08	1.90	1.89	0.99
0.2	1.49	1.51	1.01
0.4	1.30	1.30	1.00
0.6	1.23	1.23	1.00
0.8	1.19	1.19	1.00
1	1.17	1.16	1.00
10	1.11	1.07	0.96

ICRP, International Commission on Radiological Protection.

gies for Korean radiation workers [7]. The use of these energies facilitates proper interpolation of the biases over a wide energy range.

$H_p(10; E, \alpha)_{human}$ in equation (2) was calculated based on a tissue equivalent material of 30 cm × 30 cm × 2 cm positioned on the chest of the KTMAN-2. The cuboidal material is the same as that of the slab phantom, and its thickness was selected in consideration of the filter thickness of TLD. The absorbed dose was tallied in a cylindrical cell (thickness of 0.01 cm; diameter of 1 cm) defined at a depth of 10 mm (Fig. 2).

To estimate B_2, $H_p(10)$ was calculated in the same manner as B_1 (Fig. 2), and the air kerma values based on energy were calculated using the fluence-to-air kerma conversion coefficients provided in Table A.1 of the ICRU Report 47 [8]. B_2 was calculated as the ratio of the $H_p(10)/K_a$ obtained in this simulation to that provided in the ICRP Publication 74 [2].

4. Calculation of Bias-Corrected $H_p(10)$-to-Organ-Absorbed Dose Conversion Coefficients

For use in epidemiological studies, bias-corrected $H_p(10)$-to-organ-absorbed dose conversion coefficients are derived by considering the two types of biases in this study and are expressed as follows:

$$\frac{D_T}{H_p(10)} = \frac{1}{B_1 B_2}\left[\left(\frac{H_p(10)}{K_a}\right)_{slab}\right]^{-1}\left[\frac{D_T}{K_a}\right], \quad (4)$$

where $D_T/H_p(10)$ is the $H_p(10)$-to-organ-absorbed dose conversion coefficient and D_T/K_a is the air kerma-to-organ-absorbed dose conversion coefficient. We used $(H_p(10)/K_a)_{slab}$ values provided in the ICRP Publication 74 and D_T/K_a values calculated using mesh-type reference computational phantoms (MRCPs) developed based on the ICRP reference anatomical data [2, 9].

Table 2. Biases Calculated by Monte Carlo Simulation Depending on Energy and Geometry

	Energy (keV)	Bias							
		AP	PA	RLAT	LLAT	Cranial-caudal	Caudal-cranial	ROT	ISO
B_1	218	1.04	0.68	0.32	0.35	0.31	0.31	0.60	0.50
	397	1.01	0.79	0.79	0.85	0.81	0.82	0.86	0.84
	662	1.02	0.85	0.97	1.03	0.97	0.97	0.97	0.97
B_2	218	0.98	0.79	1.00	0.98	0.99	0.95	0.94	0.95
	397	0.99	0.83	1.01	0.99	1.00	0.98	0.96	0.97
	662	1.00	0.88	1.01	0.98	1.01	1.00	0.96	0.98

AP, anteroposterior; PA, posteroanterior; RLAT, right lateral; LLAT, left lateral; ROT, rotational; ISO, isotropic.

Results and Discussion

1. Simulation Verification

To verify the bias estimation method, the $H_p(10)$ values on the slab phantom were calculated using MCNP 6, and $H_p(10)/K_a$ values were compared with those of ICRP Publication 74 [2]. The $H_p(10)$ values were calculated in a cylindrical cell with a thickness of 0.01 cm and diameter of 1 cm, in the same manner as the bias calculations. The radiation field size was selected as 50 cm × 60 cm, and the fluence was 3.3×10^{-4} cm^{-2}. The photon energies ranged from 0.03 keV to 10 MeV, and 10^8 histories were considered. The $H_p(10)/K_a$ from this study and ICRP are presented in Table 1, and the differences were within 5% for all energies.

2. Quantified Biases

The quantified biases are shown in Table 2. The B_1 values, depending on the incident angle, were calculated considering the angular dependency of the personal dosimeter and differences between the slab and KTMAN-2 phantom. In AP geometry, B_1 for all energies is approximately 1, which means that the geometric differences between the two phantoms are not significant. For the AP geometry (i.e., 0°), the angular dependency is not considered in the quantification of B_1. However, although $H_p(10; E, \alpha)_{human}$ values are typically smaller than $H_p(10; E, 0°)_{slab}$ values for all energies and geometries, the B_1 values for lower energies were observed to be noticeably smaller than 1, except for the AP geometry. In addition, the magnitude of bias (i.e., the difference from 1) is larger at low energies; for example, B_1 for RLAT was 0.32 and 0.97 at 218 and 662 keV, respectively. This is because the attenuation of the incident radiation in TLD is larger for longer attenuation distances and lower energies, resulting in a relatively low response. The radiation entering the lead and plastic filters should travel longer distances as the incident angle increases. In the case of ROT and ISO geometries, the B_1 values, calculated by weighting those of other geometries, were considerably larger than those for the 75° directions (i.e., RLAT, LLAT, cranial-caudal, and caudal-cranial) because of the effects of the AP geometries.

B_2 is close to 1 for all energies and geometries except for the PA geometry, i.e., 0.79 and 0.88 at 218 keV and 662 keV, respectively. As expected, the attenuation thickness of KTMAN-2 was higher than 200 mm, whereas that of the slab phantom was only 140 mm. Therefore, the absorbed dose per unit of air kerma calculated based on KTMAN-2 was smaller than that calculated based on the slab phantom. Consequently, the calculated B_2 was also smaller in the PA geometry.

3. $H_p(10)$-to-Organ-Absorbed Dose Conversion Coefficients

For use in epidemiological studies, a library of bias-corrected $H_p(10)$-to-organ-absorbed dose conversion coefficients, $D_T/H_p(10)$, was created for three energy points, six geometries, and 30 organs (28 organs for each sex) using the biases derived in the current study and the dose coefficients provided by ICRP. The full data are tabulated in Appendices A and B. $D_T/H_p(10)$ values for energy points between the energies considered in this study can be derived by interpolation. Tables 3 and 4 show example dose conversion coefficients for adult male and female phantoms for five major organs with a tissue weighting factor of 0.12 (i.e., red bone marrow, colon, lungs, stomach, and breasts). Although most organs are exposed to the highest doses in the AP direction, the bias-corrected $D_T/H_p(10)$ values were greatest in the PA direction due to the significantly greater biases.

The practical impact of the biases on dose reconstruction can be assessed by $D_T/H_p(10)$. Ratios of $D_T/H_p(10)$ derived in the current study to those from ICRP publications without

https://doi.org/10.14407/jrpr.2022.00052

Table 3. $D_T/H_p(10)$ Conversion Coefficients with Biases Considered: Male

Organs	Energy (keV)	$D_T/H_p(10)$ (Gy/Sv)					
		AP	PA	RLAT	LLAT	ROT	ISO
Bone marrow	218	0.598	3.474	1.496	1.388	1.342	1.270
	397	0.654	2.390	0.640	0.594	0.926	0.759
	662	0.688	1.882	0.557	0.534	0.833	0.685
Colon	218	0.809	2.515	1.755	1.948	1.339	1.269
	397	0.830	1.762	0.721	0.790	0.932	0.746
	662	0.832	1.517	0.629	0.675	0.830	0.676
Lungs	218	0.704	3.171	1.249	1.273	1.284	1.284
	397	0.753	2.244	0.567	0.568	0.932	0.797
	662	0.798	1.807	0.519	0.533	0.840	0.725
Stomach	218	0.742	2.301	0.934	2.620	1.329	1.220
	397	0.793	1.683	0.455	1.047	0.888	0.727
	662	0.807	1.383	0.426	0.876	0.799	0.644
Breasts	218	0.936	1.371	2.085	2.020	1.491	1.615
	397	0.972	1.218	0.853	0.832	1.022	0.968
	662	0.976	1.144	0.716	0.713	0.912	0.842

AP, anteroposterior; PA, posteroanterior; RLAT, right lateral; LLAT, left lateral; ROT, rotational; ISO, isotropic.

Table 4. $D_T/H_p(10)$ Conversion Coefficients with Biases Considered: Female

Organs	Energy (keV)	$D_T/H_p(10)$ (Gy/Sv)					
		AP	PA	RLAT	LLAT	ROT	ISO
Bone marrow	218	0.632	3.499	1.606	1.492	1.389	1.324
	397	0.687	2.403	0.684	0.641	0.951	0.791
	662	0.715	1.890	0.596	0.570	0.855	0.706
Colon	218	0.829	2.694	1.841	1.524	1.391	1.276
	397	0.863	1.957	0.771	0.665	0.951	0.778
	662	0.859	1.569	0.658	0.599	0.851	0.682
Lungs	218	0.678	3.412	1.383	1.380	1.372	1.333
	397	0.735	2.468	0.615	0.611	0.964	0.828
	662	0.751	1.943	0.555	0.563	0.889	0.758
Stomach	218	0.782	2.805	1.117	2.903	1.440	1.342
	397	0.810	2.038	0.504	1.147	0.984	0.791
	662	0.831	1.654	0.483	0.926	0.882	0.721
Breasts	218	0.934	1.872	2.193	2.117	1.509	1.592
	397	0.964	1.551	0.928	0.891	1.047	0.949
	662	0.964	1.376	0.784	0.770	0.939	0.835

AP, anteroposterior; PA, posteroanterior; RLAT, right lateral; LLAT, left lateral; ROT, rotational; ISO, isotropic.

Table 5. Ratios of $H_p(10)$-to-Organ-Absorbed Dose Conversion Coefficients, $D_T/H_p(10)$, Derived in This Study to Those from ICRP Publications

Geometry	Ratio (this study/ICRP)		
	218 keV	397 keV	662 keV
AP	0.98	1.00	0.98
PA	1.86	1.53	1.34
RLAT	3.09	1.26	1.03
LLAT	2.93	1.19	1.00
ROT	1.78	1.22	1.07
ISO	2.10	1.23	1.06

ICRP, International Commission on Radiological Protection; AP, anteroposterior; PA, posteroanterior; RLAT, right lateral; LLAT, left lateral; ROT, rotational; ISO, isotropic.

considering the biases are shown in Table 5. Note that the differences in dose conversion coefficients arise only from the biases, and thus the ratios are equal in all organ dose coefficients. For the AP direction, the biases in the dose coefficients do not have a significant impact on the dose reconstruction. Nevertheless, the ratios (this study/ICRP) vary by exposure scenario and range from 0.98 to 3.09 for three energies and six geometries. The greatest difference in $D_T/H_p(10)$ was observed in the case of the exposure energy of 218 keV and RLAT geometry (3.09), indicating that the consideration of the biases derived in this study can result in 3.09-fold higher organ doses than those calculated using ICRP refer-

ence dose coefficients without considering the biases.

The differences in $D_T/H_p(10)$ have a significant implication for dose reconstructions for Korean industrial radiographers, whose cumulative $H_p(10)$ is highest among all Korean radiation workers [10]. In practice, an industrial radiographer who places an image film can be exposed with PA direction because the acquisition of radiographic images usually begins on the way back to the shielded area (this information was gathered in a personal conversation). In this case (i.e., 397 keV and PA direction), organ doses calculated considering the biases can be 1.53-fold higher than those without considering the biases.

Conclusion

In this study, two types of biases in organ-absorbed dose reconstruction were quantified using Monte Carlo simulations. The study demonstrated that the bias B_1, caused by personal dosimeters and calibration geometries, increases when the incident angle is large or the exposure energy is low, and B_2 is approximately 1, except for the PA geometry, which has a large difference in attenuation thickness between anthropomorphic and slab phantoms. The findings of this study indicate that the biases in $H_p(10)$ and dose coefficients ($H_p(10)/K_a$) can result in a significant underestimation of a radiation worker's dose and thus should be considered in the dose reconstruction. Moreover, this study might be used as a framework for the detailed analysis and reliable assessment of the organ-absorbed dose from occupational exposure. The application of the quantified biases to other epidemiological studies, based on new scenarios and methods, will widen the prospects of this study and is therefore of significant interest for future research.

Conflict of Interest

No potential conflict of interest relevant to this article was reported.

Acknowledgements

This work was supported by a grant given to the Korea Institute of Radiological and Medical Sciences (KIRAMS), funded by Nuclear Safety and Security Commission (NSSC), Republic of Korea (No. 50091-2021).

Author Contribution

Conceptualization: Jeong A, Kwon TE. Methodology: Jeong A, Kwon TE, Lee W. Formal analysis: Jeong A, Kwon TE. Project administration: Park S. Visualization: Jeong A. Writing - original draft: Jeong A. Writing - review and editing: Kwon TE. Approval of final manuscript: all authors.

References

1. The 2007 Recommendations of the International Commission on Radiological Protection. ICRP publication 103. Ann ICRP. 2007;37(2–4):1–332.
2. Conversion coefficients for use in radiological protection against external radiation. Adopted by the ICRP and ICRU in September 1995. Ann ICRP. 1996;26(3–4):1–205.
3. Petoussi-Henss N, Bolch WE, Eckerman KF, Endo A, Hertel N, Hunt J, et al. ICRP Publication 116: conversion coefficients for radiological protection quantities for external radiation exposures. Ann ICRP. 2010;40(2–5):1–257.
4. National Council on Radiation Protection and Measurements. Deriving organ doses and their uncertainty for epidemiologic studies (NCRP Report No. 178). Bethesda, MD: National Council on Radiation Protection and Measurements; 2018.
5. Lee C, Lee C, Park SH, Lee JK. Development of the two Korean adult tomographic computational phantoms for organ dosimetry. Med Phys. 2006;33(2):380–390.
6. Zankl M. Personal dose equivalent for photons and its variation with dosimeter position. Health Phys. 1999;76(2):162–170.
7. Kwon TE, Jeong A, Kim E, Cho J, Chung Y, Lee DN, et al. Organ dose reconstruction for Korean radiation workers study. Jeju, Korea: Proceedings of the Korean Association for Radiation Protection Spring Conference; 2021. p. 110–112.
8. International Commission on Radiation Units and Measurements. Measurement of dose equivalents from external photon and electron radiations (ICRU Report No. 47). Bethesda, MD: International Commission on Radiation Units and Measurements; 1992.
9. Yeom YS, Choi C, Han H, Lee H, Shin B, Nguyen TT, et al. Dose coefficients of mesh-type ICRP reference computational phantoms for idealized external exposures of photons and electrons. Nucl Eng Technol. 2019;51(3):843–852.
10. Park S, Seo S, Lee D, Park S, Jin YW. A cohort study of Korean radiation workers: baseline characteristics of participants. Int J Environ Res Public Health. 2020;17(7):2328.

 https://doi.org/10.14407/jrpr.2022.00052

Appendix A. Bias-Corrected $D_T/H_p(10)$ Conversion Coefficients for Male

Organs	Energy (keV)	$D_T/H_p(10)$ (Gy/Sv)					
		AP	PA	RLAT	LLAT	ROT	ISO
Bone marrow	218	0.598	3.474	1.496	1.388	1.342	1.270
	397	0.654	2.390	0.640	0.594	0.926	0.759
	662	0.688	1.882	0.557	0.534	0.833	0.685
Colon	218	0.809	2.515	1.755	1.948	1.339	1.269
	397	0.830	1.762	0.721	0.790	0.932	0.746
	662	0.832	1.517	0.629	0.675	0.830	0.676
Lungs	218	0.704	3.171	1.249	1.273	1.284	1.284
	397	0.753	2.244	0.567	0.568	0.932	0.797
	662	0.798	1.807	0.519	0.533	0.840	0.725
Stomach	218	0.742	2.301	0.934	2.620	1.329	1.220
	397	0.793	1.683	0.455	1.047	0.888	0.727
	662	0.807	1.383	0.426	0.876	0.799	0.644
Breasts	218	0.936	1.371	2.085	2.020	1.491	1.615
	397	0.972	1.218	0.853	0.832	1.022	0.968
	662	0.976	1.144	0.716	0.713	0.912	0.842
Urinary bladder	218	0.838	2.833	1.156	1.204	1.325	1.176
	397	0.862	1.944	0.542	0.542	0.888	0.715
	662	0.855	1.622	0.498	0.514	0.803	0.647
Esophagus	218	0.713	3.090	1.321	1.373	1.353	1.191
	397	0.740	2.115	0.608	0.635	0.901	0.760
	662	0.743	1.764	0.514	0.555	0.837	0.677
Liver	218	0.700	2.631	2.542	0.941	1.311	1.241
	397	0.732	1.893	1.017	0.441	0.894	0.740
	662	0.750	1.547	0.831	0.426	0.804	0.667
Thyroid	218	0.965	2.479	2.071	1.736	1.588	1.449
	397	0.985	1.840	0.853	0.725	1.067	0.854
	662	0.970	1.530	0.722	0.634	0.938	0.751
Endosteum	218	0.684	3.398	2.011	1.884	1.563	1.549
	397	0.716	2.299	0.803	0.755	1.029	0.886
	662	0.740	1.825	0.673	0.646	0.909	0.778
Brain	218	0.481	2.725	2.655	2.500	1.456	1.554
	397	0.561	1.997	1.067	1.010	1.015	0.930
	662	0.619	1.650	0.879	0.848	0.917	0.826
Salivary glands	218	0.701	3.356	2.736	2.599	1.642	1.566
	397	0.780	2.454	1.092	1.046	1.131	0.936
	662	0.819	1.992	0.894	0.868	1.009	0.825
Skin	218	0.694	3.346	2.104	2.009	1.560	1.682
	397	0.604	1.873	0.705	0.679	0.852	0.800
	662	0.508	1.213	0.488	0.477	0.619	0.568
Adrenals	218	0.404	4.083	1.086	1.096	1.276	1.150
	397	0.463	2.732	0.480	0.475	0.875	0.702
	662	0.511	2.101	0.437	0.431	0.794	0.639
Extrathoracic region	218	0.697	2.165	3.039	2.622	1.646	1.474
	397	0.782	1.615	1.173	1.143	1.115	0.848
	662	0.789	1.407	0.981	0.927	1.000	0.826
Gallbladder	218	0.699	2.382	2.785	0.951	1.285	1.180
	397	0.728	1.749	1.105	0.452	0.882	0.702
	662	0.742	1.468	0.893	0.442	0.806	0.636
Heart	218	0.775	2.645	1.306	1.803	1.319	1.261
	397	0.805	1.906	0.597	0.766	0.907	0.753
	662	0.817	1.563	0.548	0.676	0.821	0.682
Kidneys	218	0.443	4.081	1.481	1.347	1.355	1.202
	397	0.500	2.731	0.627	0.572	0.920	0.715
	662	0.544	2.094	0.551	0.515	0.825	0.646
Lymph nodes	218	0.773	2.954	1.603	1.766	1.426	1.324
	397	0.813	2.102	0.696	0.754	0.977	0.791
	662	0.823	1.698	0.613	0.663	0.874	0.706
Muscle	218	0.656	3.509	1.710	1.615	1.493	1.472
	397	0.720	2.442	0.721	0.677	1.022	0.879
	662	0.749	1.927	0.614	0.596	0.910	0.778
Oral mucosa	218	0.684	1.813	2.761	2.593	1.521	1.468
	397	0.768	1.396	1.137	1.077	1.049	0.879
	662	0.755	1.209	0.965	0.912	0.965	0.777
Pancreas	218	0.687	2.706	1.702	1.681	1.246	1.115
	397	0.720	1.945	0.734	0.718	0.856	0.670
	662	0.737	1.578	0.646	0.640	0.776	0.609
Small intestine	218	0.800	2.617	1.534	1.901	1.329	1.198
	397	0.818	1.893	0.671	0.802	0.932	0.715
	662	0.820	1.551	0.599	0.688	0.827	0.642
Spleen	218	0.470	3.895	0.473	2.034	1.332	1.253
	397	0.524	2.626	0.243	0.814	0.907	0.746
	662	0.572	2.026	0.250	0.692	0.813	0.674
Thymus	218	0.946	2.234	1.084	1.104	1.400	1.365
	397	0.972	1.709	0.483	0.494	0.958	0.822
	662	0.953	1.420	0.445	0.457	0.861	0.739
Lens of the eye	218	0.897	0.808	2.901	2.859	1.654	1.751
	397	0.952	0.778	1.168	1.159	1.142	1.018
	662	0.945	0.803	0.991	0.949	0.997	0.897
Testis	218	0.899	3.219	1.179	1.357	1.472	1.465
	397	0.915	2.388	0.569	0.629	1.015	0.867
	662	0.910	1.959	0.534	0.586	0.897	0.771
Prostate	218	0.712	3.717	1.061	1.031	1.230	1.142
	397	0.752	2.586	0.502	0.486	0.850	0.696
	662	0.771	2.021	0.474	0.462	0.770	0.633

AP, anteroposterior; PA, posteroanterior; RLAT, right lateral; LLAT, left lateral; ROT, rotational; ISO, isotropic.

Appendix B. Bias-Corrected $D_T/H_p(10)$ Conversion Coefficients for Female

Organs	Energy (keV)	$D_T/H_p(10)$ (Gy/Sv)					
		AP	PA	RLAT	LLAT	ROT	ISO
Bone marrow	218	0.632	3.499	1.606	1.492	1.389	1.324
	397	0.687	2.403	0.684	0.641	0.951	0.791
	662	0.715	1.890	0.596	0.570	0.855	0.706
Colon	218	0.829	2.694	1.841	1.524	1.391	1.276
	397	0.863	1.957	0.771	0.665	0.951	0.778
	662	0.859	1.569	0.658	0.599	0.851	0.682
Lungs	218	0.678	3.412	1.383	1.380	1.372	1.333
	397	0.735	2.468	0.615	0.611	0.964	0.828
	662	0.751	1.943	0.555	0.563	0.889	0.758
Stomach	218	0.782	2.805	1.117	2.903	1.440	1.342
	397	0.810	2.038	0.504	1.147	0.984	0.791
	662	0.831	1.654	0.483	0.926	0.882	0.721
Breasts	218	0.934	1.872	2.193	2.117	1.509	1.592
	397	0.964	1.551	0.928	0.891	1.047	0.949
	662	0.964	1.376	0.784	0.770	0.939	0.835
Urinary bladder	218	0.956	2.089	1.278	1.195	1.318	1.302
	397	0.943	1.552	0.599	0.545	0.913	0.765
	662	0.913	1.290	0.531	0.519	0.831	0.660
Esophagus	218	0.714	3.306	1.473	1.564	1.411	1.332
	397	0.753	2.311	0.622	0.629	0.966	0.790
	662	0.805	1.788	0.552	0.543	0.880	0.709
Liver	218	0.770	2.950	2.549	1.209	1.439	1.333
	397	0.801	2.089	1.023	0.547	0.977	0.791
	662	0.813	1.684	0.842	0.511	0.870	0.707
Thyroid	218	0.982	2.601	1.490	1.072	1.593	1.493
	397	1.005	1.918	0.633	0.462	1.067	0.879
	662	0.987	1.572	0.560	0.437	0.939	0.786
Endosteum	218	0.705	3.414	2.062	1.936	1.587	1.568
	397	0.736	2.312	0.822	0.772	1.048	0.898
	662	0.757	1.833	0.687	0.667	0.920	0.786
Brain	218	0.503	2.748	2.699	2.526	1.486	1.583
	397	0.581	2.010	1.086	1.022	1.034	0.949
	662	0.632	1.661	0.892	0.859	0.930	0.840
Salivary glands	218	0.639	3.382	2.875	2.732	1.697	1.543
	397	0.715	2.467	1.155	1.100	1.163	0.923
	662	0.755	1.979	0.938	0.915	1.031	0.820
Skin	218	0.698	3.389	2.158	2.036	1.579	1.697
	397	0.608	1.900	0.730	0.685	0.865	0.806
	662	0.510	1.231	0.500	0.480	0.623	0.570
Adrenals	218	0.559	3.805	1.657	1.403	1.356	1.204
	397	0.618	2.574	0.721	0.617	0.932	0.727
	662	0.651	1.997	0.629	0.564	0.833	0.662
Extrathoracic region	218	0.598	2.685	2.935	2.690	1.648	1.480
	397	0.671	2.142	1.199	1.200	1.092	0.898
	662	0.697	1.738	0.946	0.949	0.986	0.796
Gallbladder	218	0.743	2.865	2.232	1.439	1.358	1.210
	397	0.777	2.062	0.929	0.647	0.939	0.727
	662	0.788	1.657	0.778	0.600	0.840	0.657
Heart	218	218	0.792	2.935	1.480	2.211	1.428
	397	397	0.822	2.089	0.671	0.915	0.977
	662	662	0.830	1.700	0.602	0.782	0.877
Kidneys	218	218	0.580	4.049	1.706	1.598	1.441
	397	397	0.638	2.705	0.721	0.683	0.984
	662	662	0.672	2.080	0.626	0.607	0.873
Lymph nodes	218	0.757	3.065	1.708	1.647	1.433	1.331
	397	0.797	2.180	0.740	0.713	0.990	0.797
	662	0.811	1.752	0.643	0.634	0.881	0.715
Muscle	218	0.670	3.467	1.759	1.633	1.499	1.473
	397	0.728	2.416	0.740	0.689	1.028	0.879
	662	0.757	1.916	0.635	0.605	0.916	0.778
Oral mucosa	218	0.684	2.334	3.050	2.773	1.691	1.500
	397	0.757	1.889	1.211	1.129	1.124	0.891
	662	0.763	1.479	0.973	0.918	1.034	0.783
Pancreas	218	0.799	2.773	2.035	1.810	1.409	1.238
	397	0.822	1.997	0.853	0.772	0.971	0.740
	662	0.829	1.632	0.731	0.683	0.859	0.661
Small intestine	218	0.781	2.824	1.428	1.814	1.356	1.221
	397	0.810	2.063	0.639	0.760	0.927	0.734
	662	0.823	1.646	0.575	0.664	0.840	0.668
Spleen	218	0.532	4.313	0.589	2.327	1.450	1.353
	397	0.593	2.875	0.294	0.927	0.984	0.803
	662	0.636	2.199	0.297	0.780	0.878	0.714
Thymus	218	0.961	2.475	1.099	1.194	1.411	1.408
	397	0.985	1.840	0.491	0.541	0.958	0.841
	662	0.971	1.536	0.453	0.509	0.865	0.752
Lens of the eye	218	0.899	0.921	2.926	2.862	1.641	1.734
	397	0.927	0.894	1.211	1.153	1.124	1.038
	662	0.949	0.884	0.958	0.985	1.014	0.930
Ovaries	218	0.669	3.201	1.299	1.104	1.214	1.192
	397	0.720	2.194	0.570	0.504	0.837	0.702
	662	0.741	1.728	0.520	0.473	0.758	0.648
Uterus	218	0.730	3.055	1.151	1.148	1.204	1.161
	397	0.769	2.168	0.533	0.529	0.830	0.702
	662	0.786	1.737	0.491	0.495	0.762	0.637

AP, anteroposterior; PA, posteroanterior; RLAT, right lateral; LLAT, left lateral; ROT, rotational; ISO, isotropic.

https://doi.org/10.14407/jrpr.2022.00052